

Nanoscale Advances

Accepted Manuscript

This article can be cited before page numbers have been issued, to do this please use: H. K. Abid, A. B. Siddique, A. Abbas, M. A. Shaheen, A. Ali, M. Fatima, A. Shami, M. A. Alrayyani, F. A. Al-Joufi and M. A. Assiri, *Nanoscale Adv.*, 2025, DOI: 10.1039/D5NA00583C.



This is an Accepted Manuscript, which has been through the Royal Society of Chemistry peer review process and has been accepted for publication.

Accepted Manuscripts are published online shortly after acceptance, before technical editing, formatting and proof reading. Using this free service, authors can make their results available to the community, in citable form, before we publish the edited article. We will replace this Accepted Manuscript with the edited and formatted Advance Article as soon as it is available.

You can find more information about Accepted Manuscripts in the [Information for Authors](#).

Please note that technical editing may introduce minor changes to the text and/or graphics, which may alter content. The journal's standard [Terms & Conditions](#) and the [Ethical guidelines](#) still apply. In no event shall the Royal Society of Chemistry be held responsible for any errors or omissions in this Accepted Manuscript or any consequences arising from the use of any information it contains.

Biogenic synthesis of ZnO NPs, CuO NPs, and ZnO/CuO nanocomposites for facile degradation of organic pollutants and Biomedical applications

Hafiza Kainat Abid ^a, Abu Bakar Siddique ^{*a}, Azhar Abbas ^{a,b}, Muhammad Ashraf Shaheen ^c, Akbar Ali, Mashal Fatima ^a, Ashwag Shami ^e, Maymounah A. Alrayyani ^f, Fakhria A. Al-Joufi ^g, Mohammed A. Assiri ^h,

^a Institute of Chemistry, University of Sargodha, Sargodha 40100, Pakistan

^b Department of Chemistry, Government Ambala Muslim College, Sargodha 40100, Pakistan

^c Department of Allied Health Sciences, The Superior University Lahore, Sargodha-Campus 40100, Pakistan

^d Department of Chemistry, Government College University Faisalabad, 38000-Faisalabad Pakistan

^e Department of Biology, College of Science, Princess Nourah bint Abdulrahman University, P.O. Box 84428, Riyadh 11671, Saudi Arabia

^f Chemistry Department, Faculty of Science, King Abdulaziz University, Jeddah 21589, P.O. Box 80203 Saudi Arabia

^g Department of Pharmacology, College of Pharmacy, Jouf University, 72341 Aljouf, Saudi Arabia

^h Department of Chemistry, Faculty of Science, Research Center for Advanced Materials Science (RCAMS), King Khalid University, P.O. Box 960, Abha, 61421, Saudi Arabia



Abstract

The continuous increase in population and industrial activity in several areas, including textiles, leather, plastics, cosmetics, and food processing, produces harmful organic pollutants such as azo dyes, which are harmful to aquatic life and cause water pollution. The remediation of these dyes using photo-responsive metallic nanoparticles (NPs) has become a viable technique for the purification of water. This study synthesized ZnO NPs, CuO NPs, and ZnO/CuO nanocomposites using *A. nilotica* leaves extract. The NPs and NCs were characterized by UV-Vis spectroscopy, FTIR, SEM, EDX, ZP, and PXRD. All the nanomaterials showed energy bandgap in the UV and visible light region (2.15-3.00 eV) evidenced by Tauc's plots, successful capping of NPs by organic moieties, identified by FTIR, and crystallite size in the range of 13.72-16.82 nm, calculated by the PXRD data utilizing Debye-Scherrer equation and quasi spherical shape analyzed by SEM. Compared to ZnO NPs and CuO NPs, ZnO/CuO NCs showed significantly increased photocatalytic performance of 96 % for MB dye degradation and 93 % for MO dye degradation in 100 min with rate constant (k) values of about $3.35 \times 10^{-2} \text{ min}^{-1}$ and $2.65 \times 10^{-2} \text{ min}^{-1}$, respectively. The effect of catalyst dose, pH, water composition, and radical scavengers was also evaluated to optimize the conditions and propose a degradation mechanism and p-n heterojunction with fermi level shifting for improved exciton generation. The biomedical importance of the ZnO/CuO NCs was assessed by the disc diffusion assay to check the antibacterial potential, and DPPH assay, TFC assay and TPC assay for antioxidant potential. All these studies, along with the reusability of the catalyst, demonstrated the appreciable catalytic efficacy of ZnO/CuO NCs for the water purification of industrial effluents.

Keywords: metal oxide NPs, ZnO/CuO nanocomposites, green synthesis, degradation of azo dyes, effect of radical scavengers, water purification



1. Introduction

Climate change is mostly caused by environmental pollution, with industries being the most significant contributors. The textile industry's dyeing process is the leading cause of water pollution. Pollutants such as heavy metal ions, organic dyes, and microorganisms have badly affected the environment and ecosystem due to improper disposal of wastewater.¹⁻³ Synthetic dyes such as azo dyes account for approximately 65%-75% of all textile dye products. They pose a severe concern to public health due to their easy dispersion into the surrounding waterbodies and are hence considered micropollutants in aquatic environments.⁴ Textile dyes in water can inhibit oxygenation and sunlight penetration, disrupting aquatic life and photosynthesis in plants and algae.⁵

Removal of dyes and contaminants from wastewater has become more challenging in recent years.⁶ Many physical and chemical processes have been used to degrade azo dyes, such as adsorption, reverse osmosis, reductive degradation, and photocatalysis.^{7, 8} But these approaches are costly, ineffective, and require high energy. Rather, Biogenic synthesis is a non-toxic and viable method for producing NCs with enhanced photocatalytic and biological properties.^{9, 10} However, synthesizing nanomaterials utilizing microorganisms is difficult due to the complexity of isolating and maintaining cell cultures, as well as the various purification stages required. Thus, plant materials are used to synthesize NPs due to their easy availability. Also, biogenic synthesis is cost-effective and less hazardous than biosynthesis using fungal and bacterial sources.¹¹

Nanotechnology has gained popularity over the past 20 years due to the remarkable capabilities of nanomaterials, which range in size from 1 to 100 nm. These nanomaterials have been extensively



used to break down pollutants and protect the environment.¹² Zinc and copper oxides are examples of nontoxic metal oxides with various biological applications. These NPs have a large surface area, and when they are mixed, such as in a nanocomposite (NC), they result in materials with an increased surface area, larger reactive sites, higher electron and mass transfer, and improved efficiency.^{13, 14} Previously, ZnO NPs, CuO NPs, and ZnO/CuO NCs have demonstrated excellent photocatalytic properties against several organic pollutants. CuO is a p-type semiconductor having a low bandgap of 1.4 eV, whereas ZnO is an n-type semiconductor with a bandgap of 3.3 eV.¹⁶⁻¹⁸ Both of these nanomaterials have several applications in photocatalysis. ZnO/CuO NCs show excellent properties because of their p-n characteristics, high humidity sensitivity, and broad light absorption.¹⁶ However, the efficiency of these nanomaterials depends on the particles' size, shape, stability, capping agent, concentration, exposure period, biocompatibility, and pH.^{19, 20} Green synthesized metal oxide NPs and their NCs are found to be significantly more effective for antibacterial and photocatalytic applications than those of chemically synthesized nanomaterials.²¹ Therefore, an investigation of greenly synthesized heterojunction based on ZnO/CuO NCs will be an interesting aspect.

During photocatalytic reactions, the photocatalyst absorbs sunlight and degrades environmental toxins such as aquatic and atmospheric pollutants. Photodegradation has advantages over other conventional wastewater treatment technologies, as it can completely degrade organic contaminants in a few hours at room temperature. Furthermore, organic pollutants can be converted into non-hazardous products like water and carbon dioxide.²² The photodegradation of organic pollutants is facilitated in the presence of nano-catalysts under sunlight due to the generation of reactive oxygen species (ROS) in the aqueous system when NPs are exposed to sunlight.²³ In the presence of suitable light, equivalent or higher in energy than the energy bandgap,



the valence electrons of NPs are excited to the conduction band. It results in the generation of excitons (electron-hole pairs) in the system, which are actively involved in direct redox reaction with pollutants or produce secondary reactive species, like superoxide ion radicals, hydroxyl radicals, hydrogen peroxide, etc. These ROS can decompose the stable organic pollutants (i.e., azo dyes) without the addition of any additional oxidants.²⁴ However, owing to the short life of excitons, the photodegradation is severely suppressed in the case of chemically synthesized and pristine NPs. Therefore, the generation of various heterojunctions to improve the life span of excitons and more generation of ROS is an interesting area, so that activity can be enhanced and organic pollutants can be degraded easily in a shorter time. Moreover, the stability and particle size improvements are also advantageous properties of the green synthesis of heterojunctions¹⁹. Hence, the current research work has been designed for the biogenic synthesis of pristine ZnO and CuO NPs, and their heterojunction (ZnO/CuO NCs) to assess the comparative photocatalytic activities and superiority over previous reported literature.

Recently, the green synthesis of ZnO NPs, CuO NPs, and ZnO-CuO NCs has gained considerable attention due to their stability and broad-spectrum applications in photocatalysis and the biomedical field.²⁵⁻²⁷ By the capping of phytochemicals, the surface moieties of NPs greatly influence the optical properties and size of NPs.^{28, 29} Therefore, various plants are being tried to greenly synthesize metal NPs. *A. nitolica*, a plant with medicinal properties, contains various phytochemicals such as triterpenoids, flavonoids, polyphenols, terpenoids, vital oils, tannins, saponins, steroids, and fatty acids. Its primary insecticidal component, azadirachtin, has antibacterial, antiviral, and anticancer properties. Flavonoids and polyphenols like kaempferol and quercetin have anti-inflammatory, anti-cancer, and antioxidant properties. Terpenoids, such as gedunin and azadiradione, have anti-inflammatory and antifungal properties.^{30, 31} Because of the



special phytochemistry, the greenly synthesized NP and NCs are expected to be good biomedical agents. The greenly synthesized NPs have been currently used in multiple biological applications, like tissue engineering, antimicrobial coatings, targeted medication delivery, and diagnostics.³²

In this study, ZnO NPs, CuO NPs, and ZnO/CuO NCs were synthesized using *A. nilotica* leaves extract, which acts as a capping and reducing agent. These nanomaterials were successfully characterized and tested for their catalytic ability to decompose toxic dyes such as MB and MO. The effect of parameters, catalyst dose, pH, water composition, radical scavengers, and catalyst reusability was studied to check the actual wastewater treatment and deduce the degradation mechanism. Based on experimental results, a suitable heterojunction formation has been proposed for improved exciton generation. Moreover, the biological properties of the NPs have also been assessed by disc diffusion assay, DPPH assay, TFC assay, and TPC assay.

2. Experimental procedure

2.1. Materials and instruments used

The brief description of the chemicals, and instruments used has been illustrated in the supplementary information under the heading S1.

2.2. Preparation of leaf extract

The previously reported procedure was followed for the preparation of the leaf extract of *A. nilotica*.^{33, 34} Fresh *A. nilotica* leaves were washed thrice with DW to remove dust and other impurities, before being dried at ambient temperatures for 5 days. Subsequently, these leaves were crushed into fine powder with a grinder. After that, 5 g of *A. nilotica* leaf powder was mixed with 100 mL of distilled water in a round-bottom flask and stirred for 4 h at 120 °C. After filtration to remove undissolved materials, the extract was utilized to synthesize the nanomaterials. A glass



petri dish (150 mm x 15 mm) was used to dry the filtered liquid in an oven set at 50 °C. The dried plant extract was stored in an airtight jar, refrigerated at 4 °C for further work.

2.3. Preparation of ZnO NPs and CuO NPs

To prepare pristine metal oxide NPs, a 0.5 M solution of $\text{Zn}(\text{NO}_3)_2 \cdot 6\text{H}_2\text{O}$ (0.5 g in 10 mL DW) and CuCl_2 (0.6 g in 10 mL DW) was prepared in separate beakers. Then, 4 mL of plant extract was added to each salt solution at a constant temperature of 80 °C with continuous stirring at 400 rpm, respectively. To maintain the basic pH (pH = 9) of reaction mixtures, the pH of both solutions was raised by adding drops of 1 M NaOH solution after every 5-minute interval. Formation of white colored precipitates in zinc salt solution and black colored precipitates in copper salt solution indicated the preparation of NPs and hydroxides of salts. These NPs were separated using centrifugation, washed with DW, pulverized by mortar and pestle, followed by calcination at 350 °C for 3 h, which resulted in the synthesis of ZnO NPs and CuO NPs. These NPs were stored in Eppendorf tubes covered by aluminum foil and placed in a cool place to avoid exposure to sunlight.

2.4. Preparation of ZnO/CuO NCs-based heterojunction

For biogenic synthesis of ZnO/CuO NCs, 0.5 M $\text{Zn}(\text{NO}_3)_2 \cdot 6\text{H}_2\text{O}$ and 0.5 M CuCl_2 solutions were prepared in separate beakers. *A. nilotica* extract (4 mL) was gradually added to the above solutions (each solution of 110 mL) and stirred at 80 °C for 10 min. Subsequently, both solutions were combined, and pH was adjusted to 9 with constant stirring. The resulting powder was stirred for 1 h at 80 °C, cooled to room temperature, and rinsed three to four times with DW. The supernatant was removed, and the residues were oven dried (100 °C for 5 h), followed by crushing of powder and calcination at 350 °C for 3 h, resulting in the formation of a heterojunction.

2.5. Photocatalytic activity of ZnO NPs, CuO NPs, and ZnO/CuO NCs



The photodegradation of azo dyes was carried out under sunlight using biosynthesized ZnO NPs, CuO NPs, and ZnO/CuO heterojunction, following the reported literature.³⁵ To do this, 5 mg of MB and 5 mg of MO dye were dissolved in 500 mL of distilled water to obtain a 10-ppm solution for each dye in two separate beakers. 20 mL of the solution of each dye was combined with 30 mg of biosynthesized ZnO NPs, CuO NPs, and ZnO/CuO NCs. The reaction suspension was thoroughly mixed in the absence of sunlight to bring the working solution to adsorption-desorption equilibria before sunlight exposure. Afterward, the solutions were exposed to sunlight (dated: 25 June 2024) at the University of Sargodha for 100 min. The UV-visible spectra of the samples were recorded every 10 min to assess the degradation of dyes (%) using **Equation 1**.³⁶

$$\text{Degradation of azo dye (\%)} = \frac{A_0 - A_f}{A_0} \times 100 \quad (1)$$

A_0 and A_f denote the initial and final absorbance of the solution, respectively.

The degradation data were fitted to a pseudo-1st order kinetic equation (**Equation 2**) to determine rate constant values of the degradation reactions and compare the efficacies of the catalysts. The slope of the $\ln (C_0/C_t)$ vs time (t) plot was used to calculate the rate constant (k).

$$\ln \frac{C_0}{C_t} = kt \quad (2)$$

The effects of pH (3-11), catalyst dose (10-50 mg), spiked water samples of different compositions (spiked tap water (TW) from the Analytical Chemistry LAB of the University of Sargodha, spiked river water (RW) from the Jhelum River), and radical scavengers were studied to optimize the reaction conditions, real-time applications and proposal of degradation mechanism.

2.6. Biomedical applications



The antibacterial potential of the NPs and NCs was assessed by the standard disc diffusion assay, following the procedure that was reported earlier.^{5, 37} Briefly, the 2 mg/mL of each sample was sonicated in water and applied to the sterile paper disc. These discs were placed in the bacteria-seeded nutrient agar petri dishes and incubated for 24 h at 37 °C. The zone of inhibition of each disc was measured in millimeters.

For the antioxidant activity of ZnO/CuO NCs, the standard DPPH (1,1-diphenyl-2-picrylhydrazyl) assay, TFC (total flavonoid content) assay, and TPC (total phenolic content) assay were utilized, as reported in our previous work.³⁸

For the DPPH assay, the DPPH radical scavenging ability of ZnO/CuO NCs and ascorbic acid as a standard was assessed by adding different concentrations of samples (100–500 µg/mL) in 3 mL of ethanolic DPPH solution (4 mg/100 mL). After incubation for 30 min in the dark, the decrease in absorbance of solutions at λ_{max} of 517 nm was recorded and used to calculate the DPPH radical scavenging activity (%).

For the TPC assay, the various concentrations of ZnO/CuO NCs (100–500 µL; 1 mg/mL) were added to the 250 µL of 1N Folin Ciocalteu's phenol solution in 2 mL DW. Afterward, each sample was mixed with the 750 µL of 20% Na₂CO₃ solution along with the addition of 950 µL of DW. After incubation for 30 min, the absorbance of each solution was measured at 765 nm. The results of TPC assay were reported in comparison to standard gallic acid as (µg (GAE µg/mL)).

For TFC assay, the various concentrations of ZnO/CuO NCs (100–500 µL; 1 mg/mL) were mixed with 0.75 mL methanol, and the volume was raised to 2 mL by the addition of DW, followed by the addition of 300 µL of 10% AlCl₃ solution and 5% NaNO₃ solution. By increasing the volume of the mixture to 5 mL by adding 1 M NaOH solution and incubating for 40 min, the absorbance



of the samples was recorded at 510 nm. The results of TPC assay were reported in comparison to standard gallic acid as (μg (QCE $\mu\text{g/mL}$)).

2.7. Statistical treatment of data

All the photocatalytic, antimicrobial, and antioxidant experiments were performed thrice, and results have been reported as Mean \pm SD. All the results were analyzed statistically by ANOVA. Statistical significance was accepted at a level of $p < 0.05$.

3. Results and Discussion

The aqueous leaf extracts of various plants are enriched with phytochemicals, like polyphenols, terpenoids, alkaloids, etc. These bioactive compounds have the ability to reduce and stabilize the NPs, as reported by various studies.⁹ The phytochemical analysis of the aqueous leaf extract of *Acacia nilotica* was performed by various tests, as reported in literature. The qualitative phytochemical screening tests of aqueous leaf extract of *Acacia nilotica* showed the presence of phenolics, flavonoids, alkaloids, and carbohydrates in the sample, as illustrated in **Table S1**. Based on this, it was anticipated that this extract might be used as reducing and capping agent of NPs and NCs.

3.1. UV-Visible, FTIR, and Zeta potential (ZP) Analysis

Fig.1(a-c) shows the UV-Vis spectra of pristine NPs and NCs after sonication of the samples for 10 min in DW. The absorbance spectrum of aqueous extract of *A. nilotica* was also recorded and shown in **Fig. S1**. *A. nilotica* exhibits multiple UV-visible absorption peaks of almost equal absorbances in the range of 300-430 nm, while the distinct maximum absorption bands for ZnO NPs, CuO NPs, and ZnO/CuO NCs were seen at 351 nm, 327 nm, and 322 nm, respectively, as illustrated in **Fig. 1(a-c)**. The lower absorption maximum value of NCs as compared to pristine



NPs could be linked to the coupling of several metal oxide energy levels to produce a new energy level, or due to the formation of defect energy levels inside NCs.³⁹

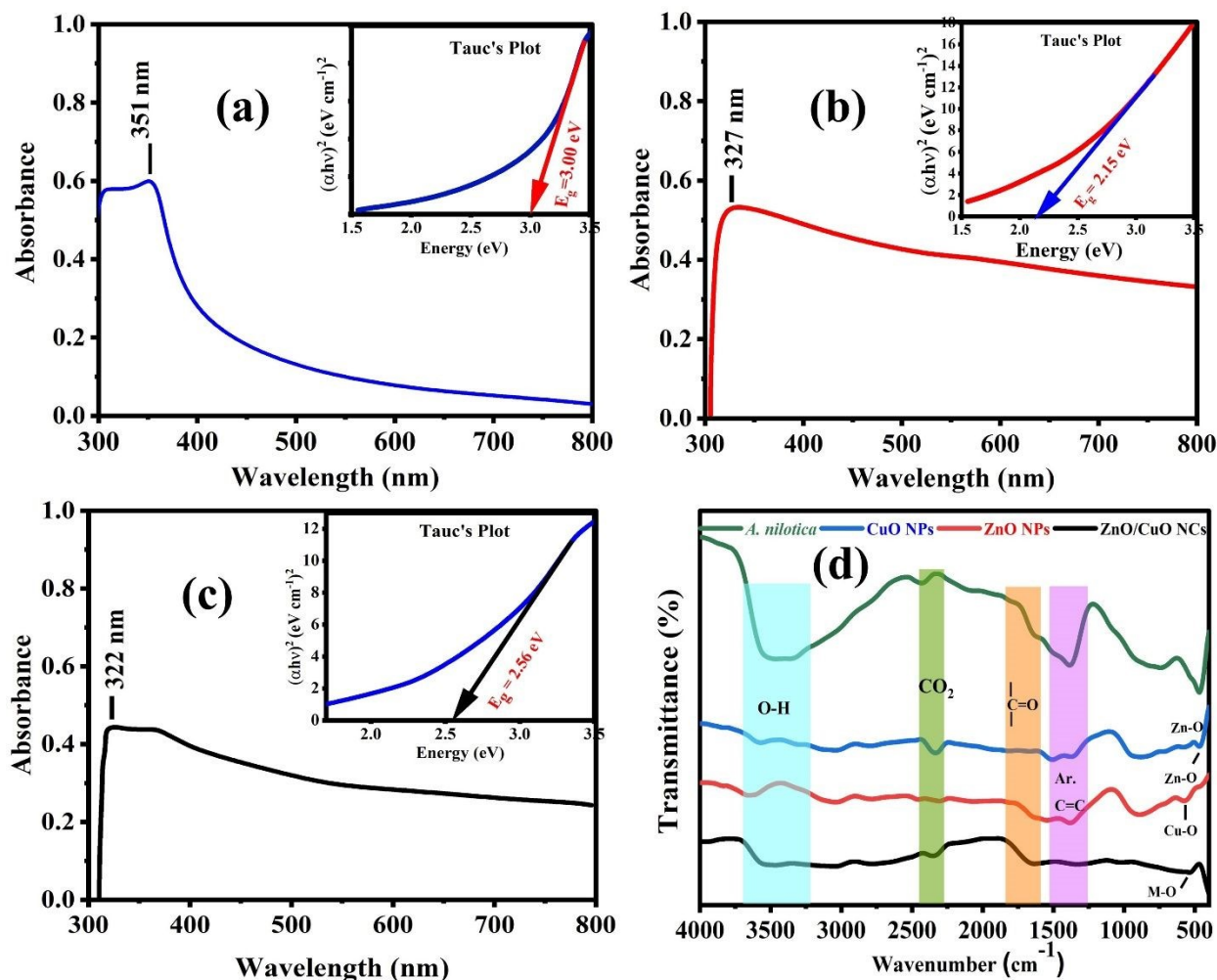


Fig. 1: UV-Vis spectra of (a) ZnO NPs (b) CuO NPs (c) ZnO/CuO NPs, (d) Comparative FTIR of extract, ZnO NPs, CuO NPs, and ZnO/CuO NCs

The optical band gap (E_g) of NPs and NCs were determined using Tauc's plot for the direct transition by extrapolating the straight line of $(\alpha h\nu)^2$ vs " $h\nu$ " graph, plotted by using Equation 3.⁴⁰

$$(\alpha h\nu)^n = A(h\nu - E_g) \quad (3)$$



Planck's constant, frequency, an energy-independent constant, the absorption coefficient, and the kind of transition are represented by α , h , ν , A , and n , respectively. The E_g values for ZnO NPs, CuO NPs, and ZnO/CuO NCs were calculated to be about 3.00 eV, 2.15 eV, and 2.56 eV, respectively, using Tauc's plot shown in the inset of each spectrum presented in **Fig. 1(a-c)**. ZnO NPs have a higher band gap as compared to ZnO/CuO NCs, indicating that increasing the amount of CuO in NCs lowers the energy band gap. For improved photocatalytic activity of NPs and NCs, the E_g must fall in the visible region, in addition to the large surface area.⁴¹ Both these properties play a decisive role in the catalytic efficacy of materials.

FTIR spectra of the samples were recorded to analyze the functional groups involved in the stabilization of pristine NPs and Zn/CuO NCs. **Fig. 1d** shows that the FTIR spectra of plant extract and biosynthesized nanomaterials were recorded in the range of 4000 to 400 cm^{-1} . The FTIR analysis revealed potential functional groups (hydroxyl, carbonyl, phenolics, etc.) involved in the reduction, capping, and production of nanomaterials. The broad band ranging from 3643-3200 cm^{-1} observed in all spectra is attributed to the O-H stretching frequency due to the presence of polyphenols on the surface and water molecules on the surface of synthesized NPs and NCs. The peaks at 1640-1730 cm^{-1} and 1480 cm^{-1} indicated the presence of the carbonyl group and aromatic C=C stretching.⁴² The peaks at 480 cm^{-1} and 523 cm^{-1} represented the Zn-O and Cu-O stretching vibrations. The FTIR spectrum of ZnO/CuO NCs displayed a peak at 538 cm^{-1} , assigned to M-O bonds, which are attributed to Zn-O and Cu-O bonds in the heterojunction.

The surface charge of the NPs and NCs significantly influences the aqueous stability and adsorption potential of the catalysts.⁴³ Larger the value of ZP, the more stable the particles in aqueous media. The more negative charge on the surface, the greater is the adsorption of cations on the surface and vice versa. Hence, the catalytic phenomenon can be comprehensively evaluated



by analyzing the ZP value. The ZP values of the biogenic synthesized NPs and NCs is depicted in **Fig. 2**. All the samples showed good stability with $ZP > -30$ mV. The ZnO NPs showed the ZP of -35.4 mV with SD of 3.2 mV, relatively better than CuO NPs ($ZP = -31.9 \pm 3.8$ mV) and ZnO/CuO NCs showed best stability with ZP value of -38.1 ± 2.2 mV. This fluctuation can be linked to the particle size variations of the NPs and NCs. Additionally, it can also be anticipated that the NCs will be highly stable with high adsorption capability for cationic dyes for photocatalytic applications.

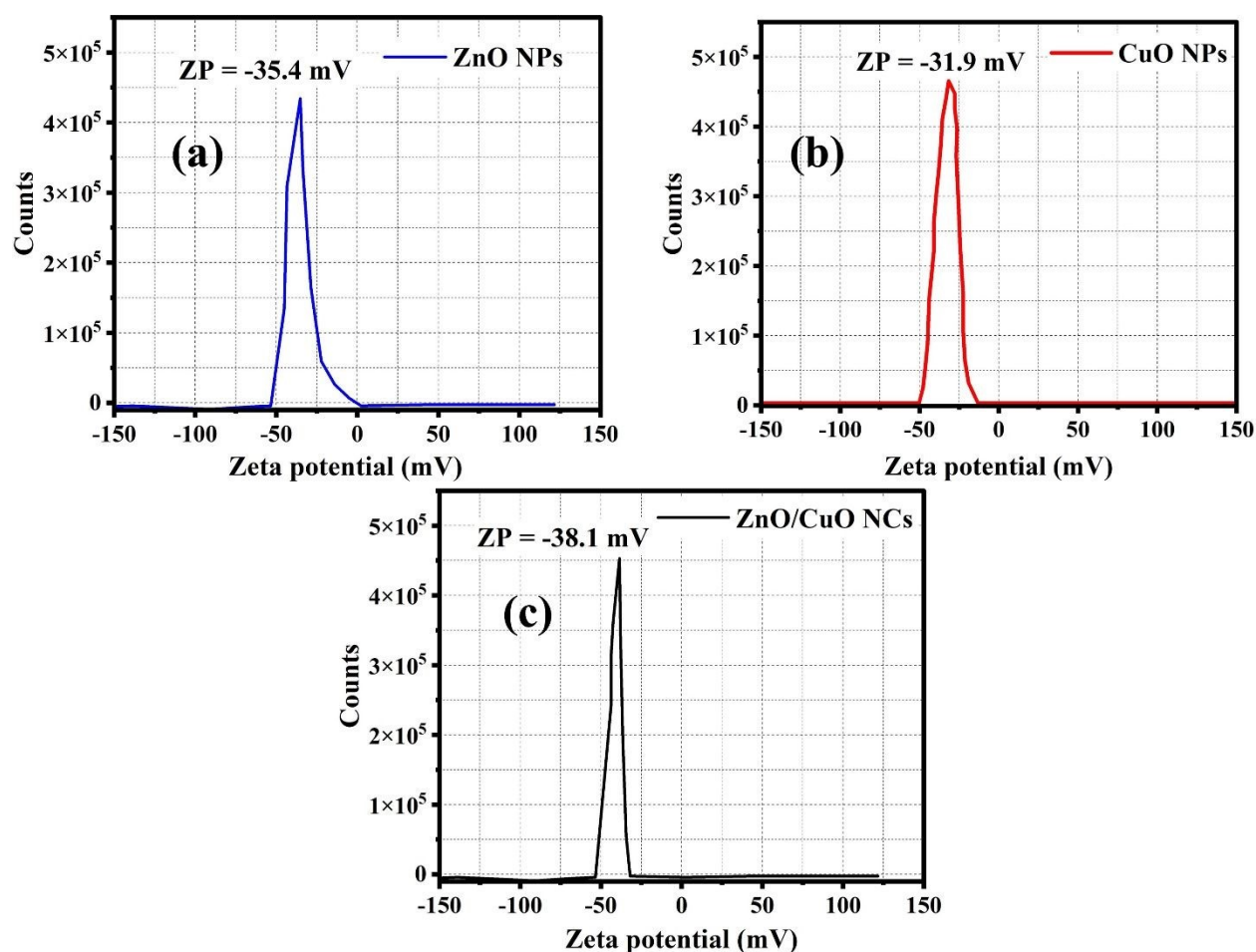


Fig. 2: ZP analysis of (a) ZnO NPs, (b) CuO NPs, and (c) ZnO/CuO NCs

3.2. PXRD Analysis



PXRD spectra were used to assess the synthesis and crystallite parameters of biosynthesized nanomaterials in the 2θ range ($30-70^\circ$). The resulting diffractograms are shown in **Fig. 3**. The ZnO NPs exhibited diffraction peaks at $2\theta = 31.94^\circ$, 34.62° , 36.42° , 47.70° , 56.71° , 62.88° , and 68.067° , which correspond to miller indices (100), (002), (101), (102), (110), (103), and (112), respectively. These findings align with the monoclinic phase of the standard JCPDS card no. 036-1451 for ZnO NPs⁴⁴. Similarly, Bragg's reflections at 2θ values of 32.97° , 35.63° , 38.77° , 48.87° , 53.51° , 58.37° , 61.68° , 66.40° and 68.18° corresponds to miller indices (110), (-111) , (111), (-202) , (020), (202), (-113) , (-311) and (220), respectively⁴⁵. These planes are well in agreement with JCPDS No. 89-2531, which confirms the formation of CuO NPs. The PXRD spectrum of ZnO/CuO NCs showed the diffraction peaks of ZnO NPs at 2θ values with lattice planes at 31.64° (100), 34.41° (002), 36.21° (101), 47.56° (102), 56.51° (110), and 62.81° (103), along with the peaks of CuO NPs at of 32.62° (110), 35.44° (-111) , 38.70° (111), and 67.86° (220). All these peaks confirmed the formation of ZnO/CuO NCs heterojunction.

The crystallite parameters were calculated by crystallographic relations, like the Debye-Scherrer, dislocation density, microstrain, and degree of crystallinity equations (**Equations 4-7**). The calculated parameters depicted in **Fig. 3** showed the smallest crystallite size of ZnO/CuO NCs (13.72 nm), in comparison to ZnO NPs (14.94 nm) and CuO NPs (16.82 nm), along with the smallest crystallinity of 29.64 % in comparison to ZnO NPs (44.35 %) and CuO NPs (69.97 %). These parameters indicated the amorphous nature of all samples and the maximum surface area of ZnO/CuO NCs due to minimum crystallinity and the smallest crystallite size.



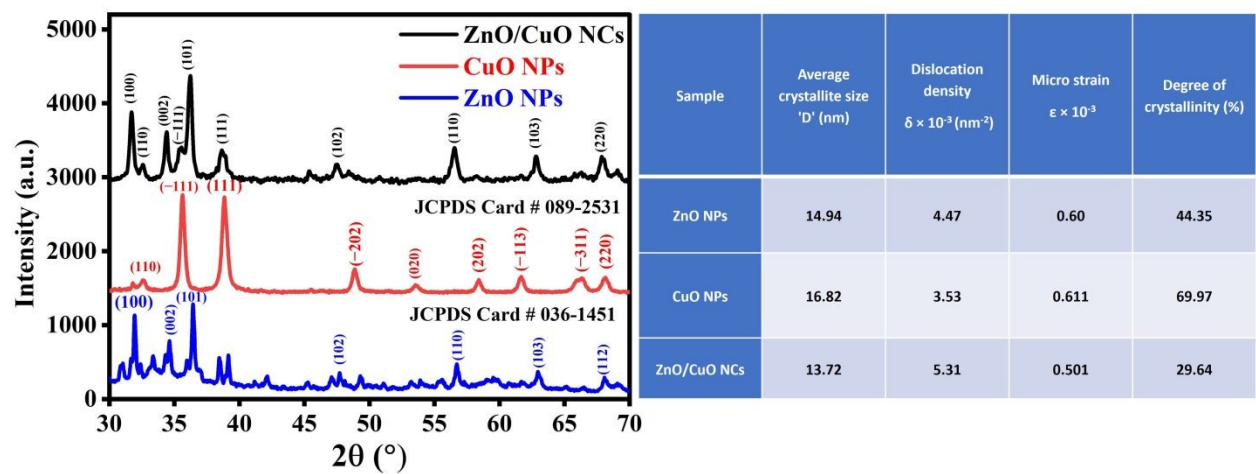


Fig. 3: PXRD spectra of nanomaterials along with the crystallite parameters of all samples

$$D = \frac{k\lambda}{\beta \cos \theta} \tag{4}$$

$$\delta = \frac{1}{D^2} \tag{5}$$

$$\epsilon = \frac{\beta}{4 \tan \theta} \tag{6}$$

$$\text{Degree of Crystallinity} = \frac{\text{Area of crystalline peaks}}{\text{Area of all peaks}} \times 100 \tag{7}$$

Here, D, k, λ, β, and θ represent crystallite size, Scherer constant or shape factor, X-ray beam wavelength, peak FWHM, and diffraction angle, respectively.

In addition to crystallite size and crystallinity (%), dislocation density and microstrain values of the samples were also calculated, which are important parameters to assess the mechanical and electrical properties. Generally, the dislocation density is inversely proportional to the crystallite size. The smaller the dislocation density, the higher the material strength and the greater the resistance to deformation under stress.⁴⁶ The highest value of dislocation density was depicted by ZnO/CuO NCs ($5.310.501 \times 10^{-3} \text{ nm}^{-2}$), which showed the low stiffness and more plastic deformations, as compared to pristine NPs. Moreover, the microstrain values indicate the level of

strain within the material, which may affect the mechanical and optical properties and electrical conductivity. The smallest value of microstrain was exhibited by ZnO/CuO NCs (0.501×10^{-3}), as compared to pristine NPs.

3.3. SEM and EDX analysis

Morphological and compositional analysis of nanomaterials was carried out by SEM and EDX, shown in **Fig. 4**. The SEM image of ZnO NPs showed that they have spherical shape morphology with little aggregations (**Fig. 4a**). They have particle size ranging from 50 to 130 nm, with average value of 83.36 ± 13.44 nm, as indicated by particle size histogram depicted in **Fig. 4b**. EDX analysis confirmed the high purity with presence of Zn and O with weight percentages of 96.76% and 3.24%, respectively (**Fig. 4c**). The oxygen peak confirms that zinc is found in its oxidized form. The EDX results verify that the ZnO NPs were successfully synthesized and their composition is in accordance with the targeted stoichiometry.

Fig. 4d shows that CuO NPs exhibit good homogeneity, a spherical form, and an adequate separation. A homogeneous distribution of particles allows the better determination of the particle size, as shown by **Fig. 4e**. The average diameter of CuO NPs was 99.63 ± 20.49 nm as calculated by plotting a histogram (**Fig. 4e**). The presence of Cu, O, C and Cl confirmed by EDX analysis with copper being a prominent constituent along with organic functional groups on surface (**Fig. 4f**).

Fig. 4g shows the shape and structure of the biosynthesized ZnO/CuO NCs using SEM with predominantly spherical shape. The average particle size was found to be 64.57 ± 12.07 nm as depicted by histogram (**Fig. 4h**). EDX analysis confirmed the presence of Cu, O, Zn, C, and Cl



(Fig. 4i). Carbon traces were visible in these three spectrums because the samples were biogenically synthesized using *A. nilotica* as the stabilizing agent.

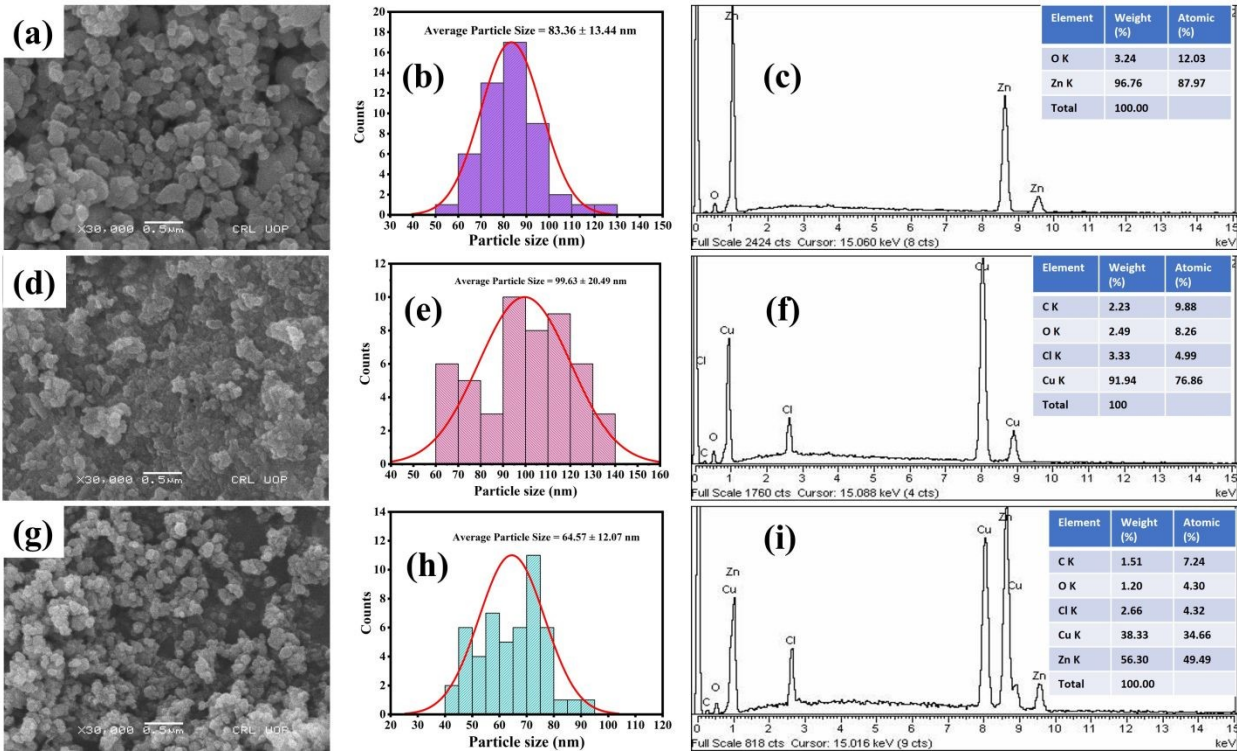


Fig. 4: (a) SEM image of ZnO NPs, (b) Particle size histogram of ZnO NPs, (c) EDX energy spectrum of ZnO NPs, (d) SEM image of CuO NPs, (e) Particle size histogram of CuO NPs, (f) EDX energy spectrum of CuO NPs, (g) SEM image of ZnO/CuO NCs, (h) Particle size histogram of ZnO/CuO NCs, (i) EDX energy spectrum of ZnO/CuO NCs

For further confirmation of the particles' morphology of ZnO/CuO NCs and their size distribution, the HR-TEM image was captured, as shown in Fig. S2(a). The HR-TEM image showed the quasi-spherical shape of the particles with an average particle size of 61.90 ± 26.12 , as depicted by the histogram (Fig. S2(b)).

In addition to the morphological analysis by HR-TEM, the surface area of the ZnO/CuO NCs (having the smallest particle size) was also estimated by Brunauer–Emmett–Teller (BET) surface



area analysis by plotting the BET isotherm, as shown in **Fig. S3**. The N₂ adsorption–desorption isotherm of the biologically synthesized ZnO/CuO NCs exhibited a hysteric loop consisting of a Type IV profile, indicating the mesoporous nature. Such porosity is essential in catalytic systems to promote surface accessibility and facilitate efficient pathways for diffusion of reactants and degradation intermediates. Based on the BET analysis, the specific surface area of the sample was 52.609 m²/g, suggesting a fairly high surface area that may be utilized in organic pollutant degradation and biomedical systems, with surface interaction being crucial. The fitting of the BET theory determined a slope of 82.3 (1/g) and an intercept of -16.10 (1/g) and a constant (C) of -4.111, consistent with multilayer adsorption and surface heterogeneity, perhaps due to the mixed-phase structure, and biogenic synthesis. Such mesoporosity, combined with nanoscale size, may result in enhanced catalytic activity of ZnO/CuO NCs for the rapid degradation of organic dyes. Accordingly, the textural properties validate the multifunctional character of the prepared material that suits well for environmental as well as biomedical purposes.

3.4. Photocatalytic activity of pristine NPs and heterojunction

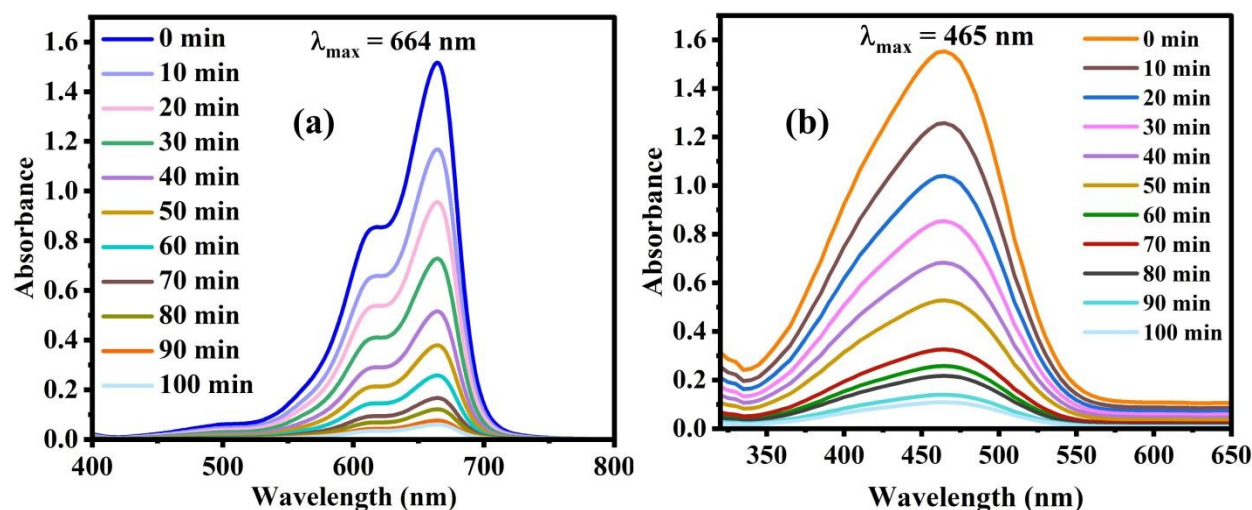
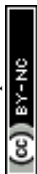


Fig. 5: Degradation spectrum of dye at different time intervals (a) MB, and (b) MO



The photocatalytic activity of biosynthesized nanomaterials was evaluated against MB and MO dyes for 100 min of visible light exposure. **Fig. 5(a-b)** shows the regular decrease in the absorbance of characteristic peaks of MB (**Fig. 5a**) and MO (**Fig. 5b**) after intervals of every 10 minutes. Using the absorbance values of characteristic peaks, the time-dependent photodegradation (%) of dyes using nanomaterials was measured using **Equation 1**. The results showed that MB and MO dyes rapidly degraded as exposure time increased for all samples until they became colorless or faded. The degradation efficiencies (%) measured were $96.0 \pm 1.5\%$, $78.2 \pm 1.0\%$, $63.1 \pm 1.4\%$ for MB dye (**Fig. 6a**) and $93.1 \pm 1.25\%$, $78.3 \pm 0.8\%$, $63.1 \pm 1.3\%$ for MO dye (**Fig. 6b**) by ZnO/CuO NCs, ZnO, and CuO NPs, respectively. Change in MB and MO dye color and resulting degradation (%) was more noticeable in the presence of NCs than in pristine NPs. This can be anticipated due to the creation of a heterojunction by mixing of oxides, which may significantly reduce the recombination of excitons and increase the visible region's photo-responsive range. To further understand the degradation process, kinetic investigations of the reaction were also conducted by fitting the degradation data into a pseudo-first-order kinetics equation, following **Equation 2**.

The kinetics data showed that the NCs samples had significantly higher photocatalytic degradation rates than ZnO NPs and CuO NPs, as depicted in **Fig. 6(c-d)**. The rate constant values for ZnO/CuO NCs, ZnO NPs, and CuO NPs were calculated to be $3.35 \times 10^{-2} \text{ min}^{-1}$, $1.49 \times 10^{-2} \text{ min}^{-1}$, and $1.08 \times 10^{-2} \text{ min}^{-1}$, respectively, for MB dye (**Fig. 6c**) and $2.65 \times 10^{-2} \text{ min}^{-1}$, $1.46 \times 10^{-2} \text{ min}^{-1}$, and $1.01 \times 10^{-2} \text{ min}^{-1}$, respectively, for MO dye (**Fig. 6d**).



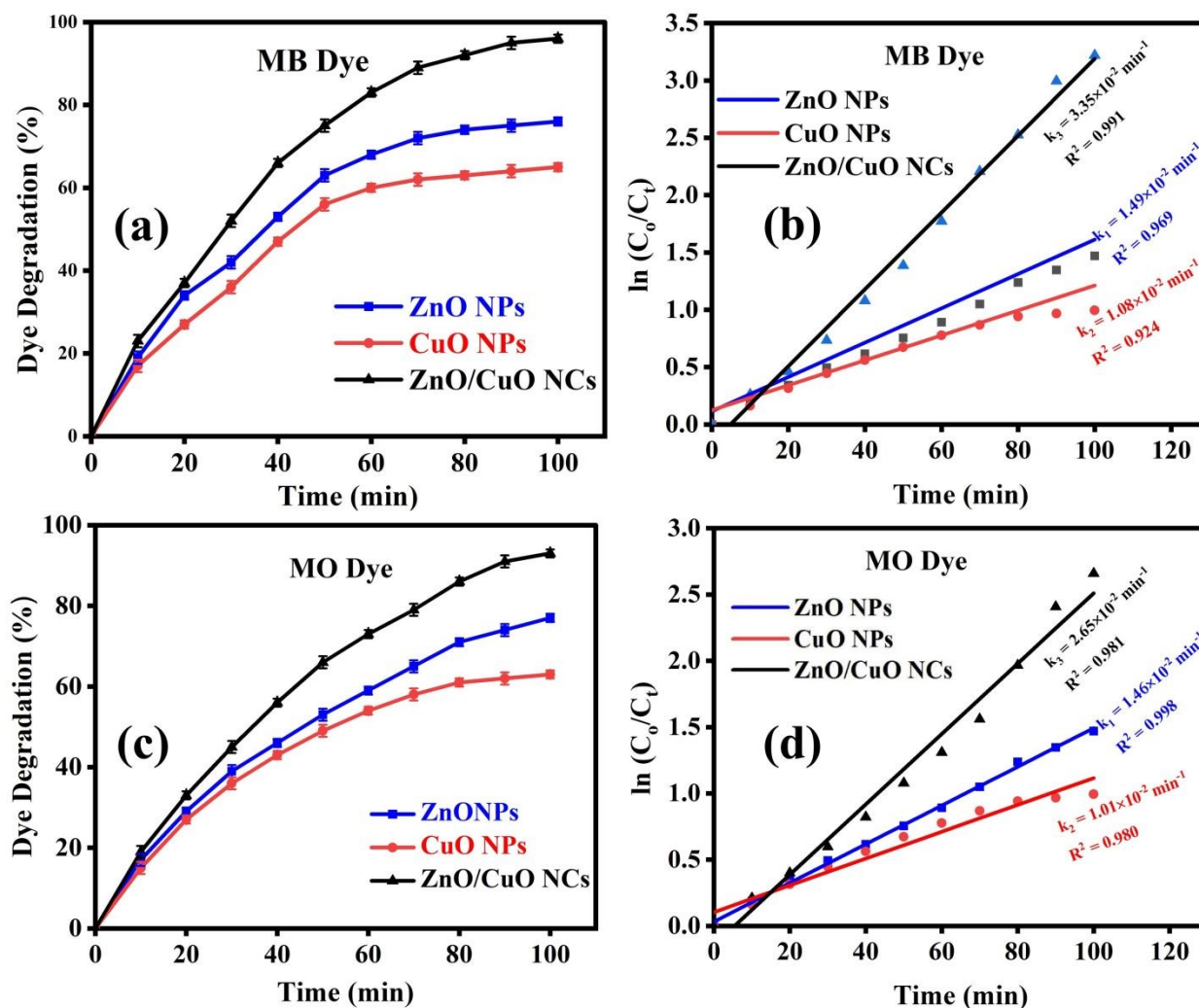


Fig. 6: Degradation efficiency versus time for (a) MB dye, (b) MO dye, (c) the reaction kinetics of MB dye (d) the reaction kinetics of MO dye. All results have been reported as Mean \pm SD, with number of replicates (n) = 3. Statistical significance was accepted at a level of $p < 0.05$.

3.5. Effect of reaction variables on the catalytic efficiency of samples

The photocatalytic efficiency of the catalyst is greatly influenced by the reaction conditions, like catalyst dose, pH, matrix composition, and ROS inhibiting compounds. For the real sample analysis, reaction condition optimization, and proposed degradation mechanism, the catalyst



efficiency was analyzed at various catalyst dosages, pH, water samples, and ROS inhibitors, by following the same method described earlier.¹

The effect of ZnO/CuO NCs dose (as depicted in Fig. 7a) showed that the catalytic efficiency increased with the increase in catalyst amount from 10 mg to 30 mg, due to the increase in surface area and active sites available for adsorbing dye molecules. With the further increase of ZnO/CuO NCs dose (above 30 mg), the dye degradation (%) was reduced gradually, which might be due to an increase in turbidity of the suspension, resulting in light scattering from surfaces and less penetration of light inside the reaction mixture to generate the excitons.

The effect of pH (depicted in **Fig. 7b**) showed anomalous behavior for MB and MO dye. With the increase of pH from 3 to 7, the catalytic activity of ZnO/CuO NCs was increased due to easy adsorption of cationic dye molecules on the surface and less inhibition of radicals by H⁺ ions near neutral pH. With further increase of pH (at pH 9 and 11), the degradation efficiency was decreased because the hydrolysis of the catalyst may occur at high pH, resulting in the reduction of surface area and active sites. While in the case of MO, the same trend of degradation was observed at pH 9 and 11, however, below pH 7, the ZnO/CuO NCs showed better degradation of MO than MB. This trend was observed because the MO is anionic in nature, and its adsorption efficiency was increased with the decrease of surface negative charge, however, the overall reduction was observed due to inhibition of ROS by high h⁺ concentration.

The effect of various water compositions (**Fig. 7c**) showed the maximum dye degradation (%) in spiked DW due to the absence of any interferences. However, with the increase of hardness and impurities in spiked water samples, the degradation (%) was continuously reduced, as depicted by more degradation (%) of spiked RW than spiked TW.



The effect of initial concentration of dyes on the photodegradation ability of the ZnO/CuO NCs was studied to optimize the reaction conditions and degrade high concentrations of dyes. The results of the experiments (**Fig. 7d**) showed the gradual decrease in the catalytic efficiency of ZnO/CuO NCs with the increase of dye concentration. This decrease in degradation (%) in the given time (100 min) was observed due to the limited number of active sites on the catalysts' surface for the generation of ROS, resulting in the slower degradation of dye solutions. The decrease in degradation (%) may also be observed due to an increase in turbidity of the mixture, resulting in less penetration of light for the photodegradation reaction on the catalyst surface.

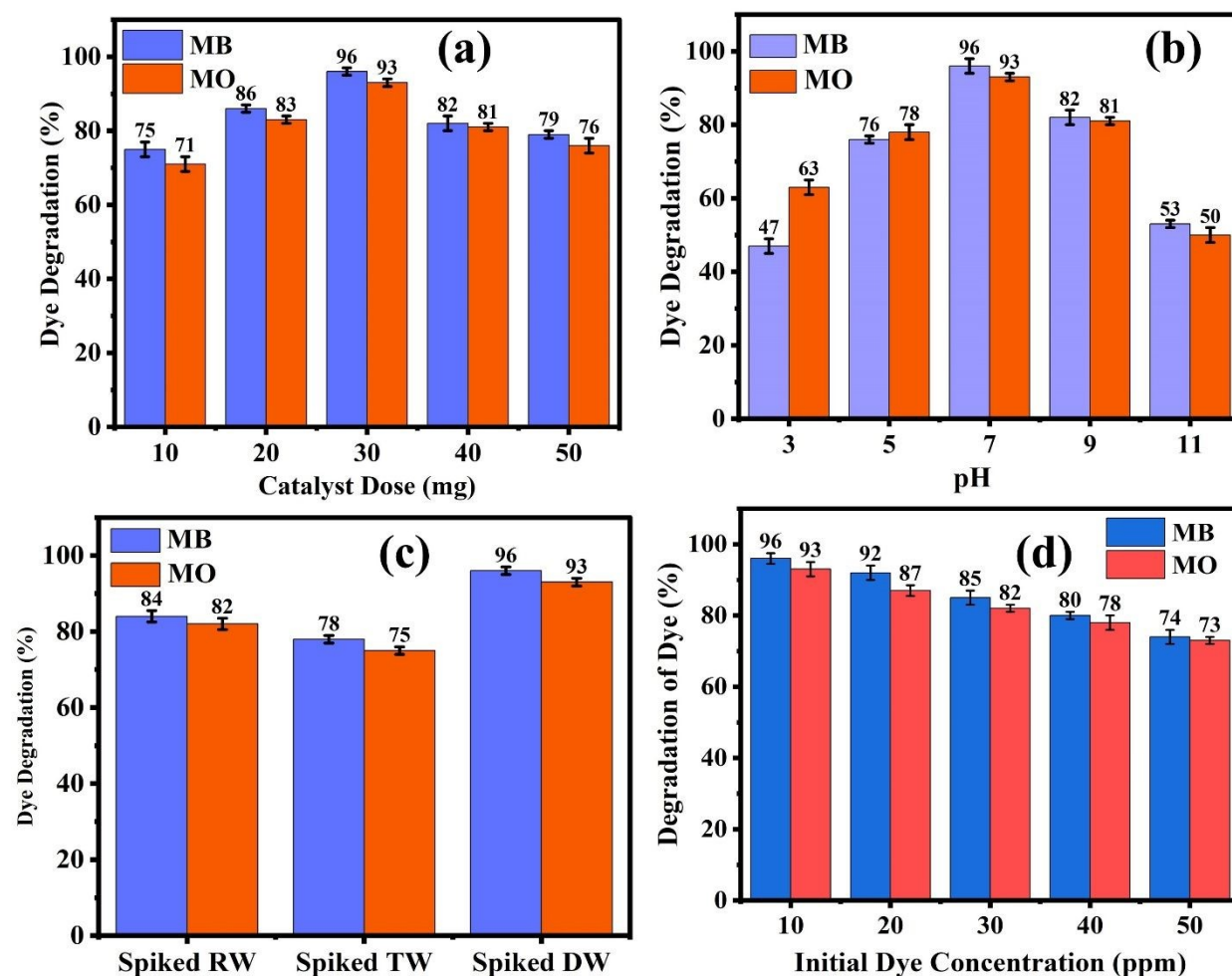


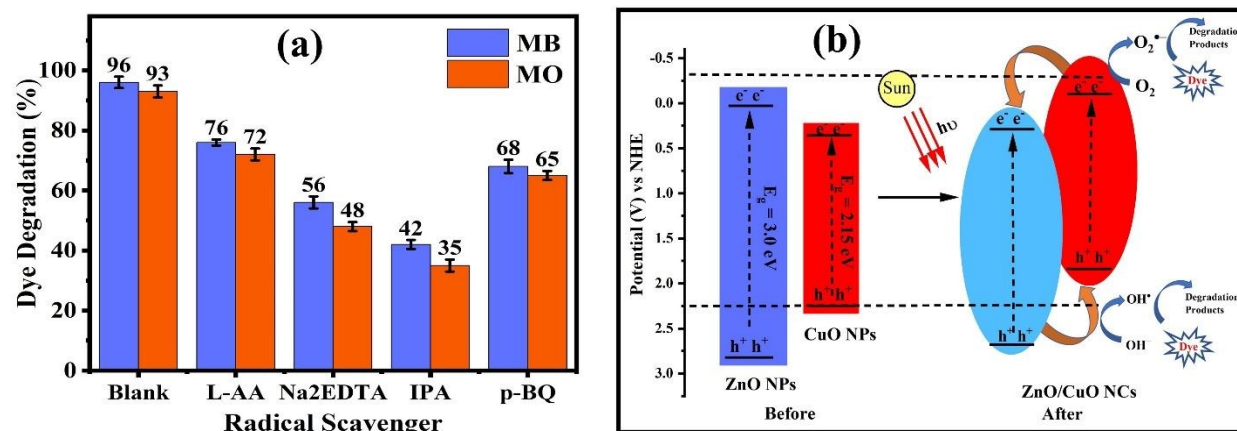
Fig. 7: Effect on dye degradation at various (a) catalyst dose, (b) pH, (c) water matrix, and (d) Initial dye concentration. All results have been reported as Mean \pm SD, with number of replicates (n) = 3. Statistical significance was accepted at a level of $p < 0.05$.

The effect of radical scavengers (**Fig. 8a**) showed minimum involvement of superoxide ($O_2^{\bullet-}$) and hydrogen peroxide (H_2O_2) in the degradation process because minimum inhibition of dye degradation (%) was observed in presence of L-ascorbic acid (L-AA)- acts as H_2O_2 scavenger, and p-benzoquinone (p-BQ)- acts as $O_2^{\bullet-}$ scavenger, while in presence of isopropanol (IPA)- acts as $\bullet OH$, the maximum inhibition of degradation (%) was observed followed by Na_2EDTA -acts as h^+ scavenger. These results indicated the generation of all ROS in the reaction mixture and their active involvement in degradation. A degradation mechanism has been proposed based on these observations, as shown by **S2** in the supplementary information.

Based on the experimental evidence and theoretical calculations of band edge potentials (valence band (E_{VB}) and conduction band (E_{CB})) of ZnO NPs and CuO NPs ²², it was suggested that there was a shifting of Fermi levels of ZnO NPs and CuO NPs, as shown by **Fig. 8b**. The Fermi level of ZnO NPs is lowered, and CuO NPs is shifted upward on formation of a p-n heterojunction. As a result, the generation of $O_2^{\bullet-}$ and H_2O_2 is also facilitated in addition to the generation of $\bullet OH$ and h^+ . This shifting of Fermi levels also facilitated the better absorption of sunlight. It lowered the recombination rate of electron-hole pairs, resulting in better photocatalytic activity of ZnO/CuO NCs heterojunction for the degradation of azo dyes. ¹⁴ Moreover, the photocatalytic superiority of the synthesized ZnO/CuO NCs was also emphasized by the comparison with the degradation rate constants of the previously reported materials, depicted in Table S2. The comparison table showed the improved photocatalytic potential of the ZnO/CuO NCs, as indicated by high degradation constant values for azo dyes under sunlight. Hence, the current work has successfully reported the



ZnO/CuO NCs as improved photo-responsive photocatalysts for the remediation of azo dyes and water purification of industrial effluents.



3.6.Fig. 8: (a) Effect of radical scavengers on dye degradation; (b) Schematic illustration of band edge positions of E_{VB} and E_{CB} of ZnO NPs and CuO NPs, and proposed band alignment after formation of p-n heterojunction (ZnO/CuO NCs). All results have been reported as Mean \pm SD, with number of replicates (n) = 3. Statistical significance was accepted at a level of $p < 0.05$.

3.7.Total organic carbon (TOC) analysis and reusability studies

The complete photodegradation of azo dyes to carbon dioxide and water, termed as mineralization under sunlight, is accomplished through a complex pathway. The color of the solution fades when the azo bond is broken down; however, the complete mineralization of the solution is a slow process and proceeds swiftly by completely degrading the organic species to water and carbon dioxide. The incomplete degradation may result in the generation of more reactive or toxic species, which may further deteriorate the water quality. Therefore, the TOC removal analysis of the azo dye solution was carried out to assess the extent of mineralization. The TOC removal (%) vs time



plot (**Fig. 9a**) depicted the 83% and 82 % mineralization of MB and MO dyes, respectively, after an exposure time of 4 h. These results demonstrated that the proposed catalyst (ZnO/CuO NCs) can effectively mineralize the azo dyes under sunlight and can be utilized to purify the water after long-term exposure, in contrast to only the disappearance of color of the solution.

For reusability studies, the ZnO/CuO NCs with improved sunlight absorbance and photocatalytic performance were evaluated to degrade MB and MO spiked DW samples for five consecutive cycles batchwise. After each cycle, the ZnO/CuO NCs were recovered from the mixture by centrifugation, followed by drying in an oven at 80 °C for 3 h. The reusability studies showed a meager decrease in activity (~9 %) after five cycles, as depicted by **Fig. 9b**. These observations proved the stability and reusable nature of the proposed catalyst with minimum effect on activity.

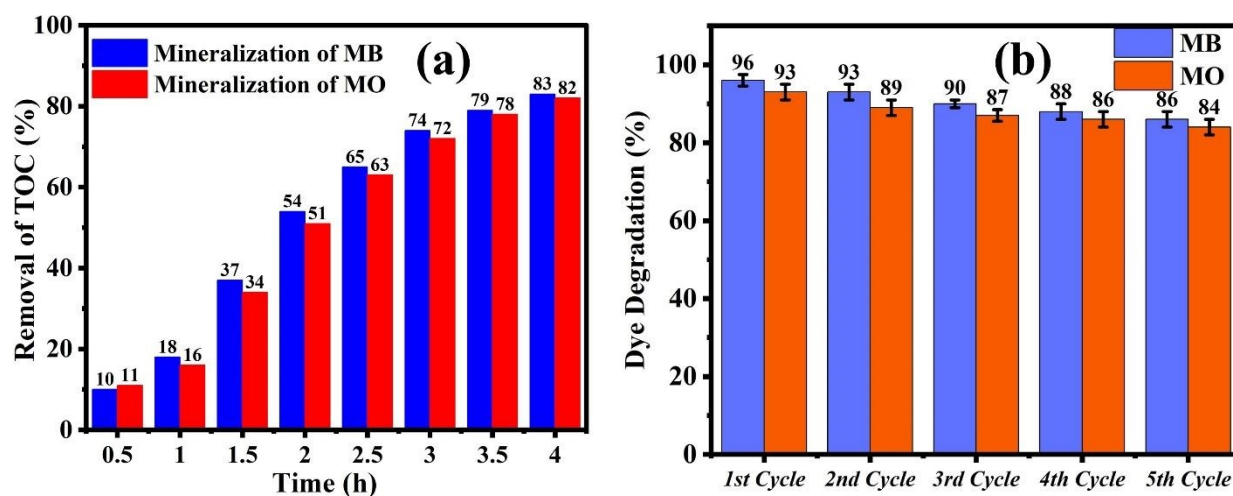


Fig. 9: (a) Removal of TOC (%) with time, (b) Reusability studies of ZnO/CuO NCs to degrade azo dyes in spiked DW. All results have been reported as Mean \pm SD, with number of replicates (n) = 3. Statistical significance was accepted at a level of $p < 0.05$.



To verify the stability of the ZnO/CuO NCs after the 5th cycle of use, the post-usage SEM, particle size histogram by SEM, and FTIR analysis of the sample were recorded, as shown in **Fig. S4**. The SEM analysis revealed well-separated NPs with a quasi-spherical morphology, having an average particle size of 79.51 ± 10.75 nm, as shown in **Figures S4a** and **S4b**, respectively. The slight increase in size was observed due to a small agglomeration of the particles after several uses, which might be responsible for the slight decrease in photocatalytic activity after five uses. To compare the surface functionalities of the NCs, the FTIR spectrum of the sample was compared before and after usage, as shown in **Fig. S4(c)**. The comparative spectrum showed that retention of almost all functional groups on the surface of NCs occurred even after five uses. These studies highlighted the potential of the synthesized material for repeated use.

Biomedical Applications

The disc diffusion assay results (depicted in **Fig. 10a**) showed the more vulnerable nature of gram-positive bacterial strains (*L. monocytogenes* and *S. epidermidis*) than gram-negative bacteria (*P. aeruginosa* and *B. bronchiseptica*) by NPs and NCs. This activity trend can be attributed to the variation in the membrane barriers of both strains. Since the gram-positive bacteria have a thick peptidoglycan layer surrounding the cytoplasmic membrane. In contrast, the gram-negative bacteria have lipopolysaccharide in the outer leaflet and a thin layer of peptidoglycan on the inner side; hence, it can be postulated that the NPs and NCs have less interaction with lipopolysaccharide than peptidoglycan, resulting in better activity against gram-positive bacteria. Although the exact mechanism of action of NPs against microbes is still unknown, however it has been reported earlier that the NPs inhibit bacterial growth by crossing the membrane barriers and interacting directly with the enzymes and genetic material, as well as by producing ROS in the vicinity and inside the bacteria.^{1, 47} The maximum inhibition of bacterial colonies by ZnO/CuO



NCs (comparable to standard erythromycin) can be attributed to the smallest particle size and the easy generation of ROS compared to other nanomaterials.

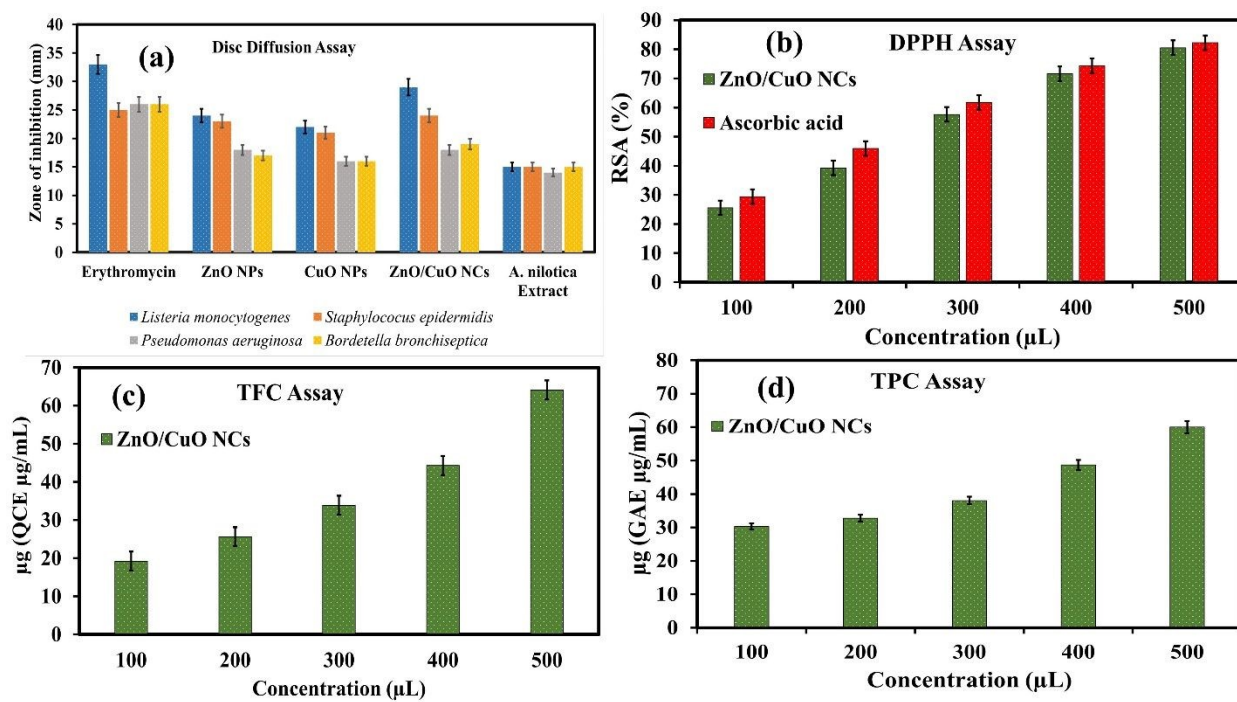


Fig. 10: Biological activities results of: **(a)** Disc diffusion assay, **(b)** DPPH assay, **(c)** TFC assay, and **(d)** TPC assay. All results have been reported as Mean \pm SD, with number of replicates (n) = 3. Statistical significance was accepted at a level of $p < 0.05$.

The antioxidant activity of the ZnO/CuO NCs, assessed by the DPPH assay (**Fig. 10b**), TFC assay (**Fig. 10c**), and TPC assay (**Fig. 10d**), showed a gradual increase with the rise in concentration from 100 μ L to 500 μ L. The DPPH assay results showed that the radical scavenging ability (RSA (%)) became almost equal to that of standard ascorbic acid ($80.3 \pm 1.5\%$) at a concentration of 500 μ L, as shown in **Fig. 10b**. The highest TFC value of 64.0 ± 1.1 μ g (QCE μ g/mL) was obtained in comparison to the highest TPC value of 60.0 ± 1.3 μ g (GAE μ g/mL), as shown in **Fig. 10c and 10d**, respectively. This appreciable antioxidant activity of ZnO/CuO NCs was attributed to the capping



of biologically active metabolites (phenolics, flavonoids, terpenoids etc.) on the surface of NCs that synergistically enhance the antioxidant activity.³⁸

4. Conclusion

The biogenic synthesis of pristine and ZnO/CuO NCs-based heterojunction using *A. nilotica* has been reported as a cost-effective and eco-friendly photocatalyst for the remediation of organic pollutants. These nanomaterials were characterized by UV-Vis, FTIR, PXRD, ZP, SEM, and EDX analysis. UV-Vis spectra revealed improved sunlight absorption and better exciton separations in ZnO/CuO NCs than pristine ZnO NPs and CuO NPs. FTIR showed the characteristic peaks of M-O bonds ($490\text{--}540\text{ cm}^{-1}$) and several functional groups (hydroxyl, carbonyl, aromatic rings, etc.) on the surface of nanomaterials as a capping agent. PXRD spectra revealed the characteristic diffraction lines of ZnO NPs, CuO NPs, and ZnO/CuO NCs with average crystallite sizes of 14.94 nm, 16.82 nm, and 13.72 nm, respectively. SEM analysis revealed the spherical shapes of NPs and NCs with particle diameters of $83.36\pm13.44\text{ nm}$, $99.63\pm20.49\text{ nm}$, and $64.57\pm12.07\text{ nm}$ for ZnO NPs, CuO NPs, and ZnO/CuO NCs, respectively. When exposed to sunlight, these ZnO NPs, CuO NPs, and ZnO/CuO NCs showed good photocatalytic efficacy in degrading harmful azo dyes, like MB and MO. The degradation for MB dye was found to be $96.0\pm1.5\%$, $78.2\pm1.0\%$, and $63.1\pm1.4\%$ for ZnO/CuO NCs, ZnO NPs, and CuO NPs, with rate constant values of $3.35\times10^{-2}\text{ min}^{-1}$, $1.4\times10^{-2}\text{ min}^{-1}$, and $1.0\times10^{-2}\text{ min}^{-1}$, respectively. Similarly, degradation (%) for MO dye was found to be $93.1\pm1.25\%$, $78.3\pm0.8\%$, and $63.1\pm1.3\%$, with rate constant values of $2.65\times10^{-2}\text{ min}^{-1}$, $1.4\times10^{-2}\text{ min}^{-1}$, and $1.0\times10^{-2}\text{ min}^{-1}$ for ZnO/CuO NCs, ZnO NPs, and CuO NPs, respectively. The effect of reaction parameters showed the maximum degradation of dyes at a catalyst dose of 30 mg and pH 7 in spiked DW, along with the maximum inhibition of degradation in the presence of $\cdot\text{OH}$ and h^+ scavengers. A suitable degradation mechanism and generation of p-



n heterojunction were proposed based on radical scavenging experiments. Reusability experiments confirmed the stable and reusable nature of ZnO/CuO NCs for wastewater treatment applications. Conclusively, the proposed heterojunction-based photocatalyst can be optimized for commercial-scale applications with improved degradation capability under sunlight. Moreover, the biological evaluation of the ZnO/CuO NCs showed better inhibition of bacterial strains than pristine ZnO NPs and CuO NPs, as well as the extract. The antioxidant activity results showed the DPPH radical inhibition (%) of 80.3 ± 1.5 , TFC of 64.0 ± 1.1 μg (QCE $\mu\text{g/mL}$), and TPC of 60.0 ± 1.3 μg (GAE $\mu\text{g/mL}$) by ZnO/CuO NCs. All these activities demonstrated the potential of these NCs for biomedical applications.

CRedit Author Statement

H. K. Abid & A. B. Siddique: Methodology, Investigation, Writing –original draft, Writing – review & editing. **A. Abbas, M. A. Shaheen, & A. Ali:** Conceptualization, Supervision, Writing – review & editing. **Mashal Fatima, Ashwag Shami, Maymounah A. Alrayyaniv, & Fakhria A. Al-Joufi:** Investigation, Writing – review & editing. **Mohammed A. Assiri:** Writing – review & editing.

Acknowledgment

The authors express their gratitude to Princess Nourah bint Abdulrahman University Researchers Supporting Project number (PNURSP2025R31), Princess Nourah bint Abdulrahman University, Riyadh, Saudi Arabia. The authors express their appreciation to the Deanship of Scientific Research at King Khalid University, Saudi Arabia, for this work through a research group program under grant number RGP-2/673/46.

Competing Interests



The authors have no known financial or non-financial interests to disclose.

Availability of data and materials

All evaluated data is available in the manuscript. Additional information/data can be provided upon reasonable request.

References

1. H. Ahmad, A. B. Siddique, S. Zaheer, R. Sattar, A. Abbas, M. Amin, R. Al-Salahi, H. A. Abuelizz and M. Z. Saleem, *Journal of Water Process Engineering*, 2025, **74**, 107855.
2. A. Abbas, A. B. Siddique, R. Batool, M. Sher, M. I. Irfan and M. A. Abbas, *Starch-Stärke*, 2023, **75**, 2200191.
3. F. Khan, A. B. Siddique, M. I. Irfan, M. N. u. Hassan, M. Sher, H. A. Alhazmi, A. N. Qramish, H. M. Amin, R. Qadir and A. Abbas, *Water, Air, & Soil Pollution*, 2024, **235**, 536.
4. A. B. Siddique, M. A. Shaheen, S. Shafeeq, A. Abbas, Y. Zaman, Z. Ishaque and M. Aslam, *Materials Advances*, 2025.
5. A. B. Siddique, M. A. Shaheen, A. Abbas, Y. Zaman, M. Z. Ishaque, A. Shami, M. Aslam, K. M. Alsyaad and A. Ali, *Journal of Molecular Structure*, 2025, **1331**, 141566.
6. A. Rafiq, M. Ikram, S. Ali, F. Niaz, M. Khan, Q. Khan and M. Maqbool, *Journal of Industrial and Engineering Chemistry*, 2021, **97**, 111-128.
7. R. Sattara, M. Rasoola, R. Qadirb, A. Siddiqueb, M. Irfanb, I. Sabac, M. Akhtarb, M. ur Rehmana and M. Mustaqeemb, *Journal of Optoelectronic and Biomedical Materials Vol*, 2023, **15**, 1-9.



8. M. I. Irfan, M. Sadiq, L. Zohra, A. B. Siddique, M. Yousaf, M. Rubab, K. Urooj, A. Aziz, H. Ali and M. Fatima, *Journal of Water Process Engineering*, 2024, **68**, 106337.
9. A. B. Siddique, M. A. Shaheen, A. Abbas, Y. Zaman, M. U. Rasheed, A. Karim, M. Mustaqeem, M. M. Alam and A. S. Alahmari, *Water, Air, & Soil Pollution*, 2025, **236**, 1-22.
10. G. Murugadoss, R. K. Manavalan, N. Venkatesh, G. Thiruppathi, P. Sundararaj, D. Murugan and K. Kirubaharan, *Materials Science and Engineering: B*, 2025, **316**, 118148.
11. X. Zhang, S. Yan, R. Tyagi and R. Surampalli, *Chemosphere*, 2011, **82**, 489-494.
12. J. S. Shukla, *Environmental Applications of Nanotechnology*, Academic Guru Publishing House, 2024.
13. A. B. Siddique, M. A. Shaheen, A. Abbas, Y. Zaman, M. A. Bratty, A. Najmi, A. Hanbashi, M. Mustaqeem, H. A. Alhazmi and Z. ur Rehman, *Heliyon*, 2024, **10**, e40679.
14. P. Nayak, S. Kumar, I. Sinha and K. K. Singh, *Environmental Science and Pollution Research*, 2019, **26**, 16279-16288.
15. A. A. M. Sakib, S. M. Masum, J. Hoinkis, R. Islam and M. A. I. Molla, *Journal of Composites Science*, 2019, **3**, 91.
16. R. Saravanan, S. Karthikeyan, V. Gupta, G. Sekaran, V. Narayanan and A. Stephen, *Materials Science and Engineering: C*, 2013, **33**, 91-98.
17. N. Abraham, C. Unni and D. Philip, *Journal of Materials Science: Materials in Electronics*, 2018, **29**, 21002-21013.
18. M. Tariq, Y. Zaman, M. Shahzad, K. Ahmad, A. B. Siddique and H. Zaman, *Materials Science and Engineering: B*, 2023, **294**, 116549.
19. M. Jeevarathinam and I. Asharani, *Scientific Reports*, 2024, **14**, 9718.



20. V. U. Siddiqui, A. Ansari, M. T. Ansari, M. K. Akram, W. A. Siddiqi, A. M. Alosaimi, M. A. Hussein and M. Rafatullah, *Catalysts*, 2021, **11**, 1509.
21. A. G. Bekru, L. T. Tufa, O. A. Zelekew, M. Goddati, J. Lee and F. K. Sabir, *ACS omega*, 2022, **7**, 30908-30919.
22. A. B. Siddique, M. A. Shaheen, A. Abbas, Y. Zaman, A. Ali, M. Naeem-ul-Hassan and J. Iqbal, *Journal of Environmental Chemical Engineering*, 2024, **12**, 112725.
23. K. Madeshwaran and R. Venkatachalam, *Journal of Industrial and Engineering Chemistry*, 2024, **140**, 454-467.
24. D. Thatikayala and B. Min, *Journal of Materials Science: Materials in Electronics*, 2021, **32**, 17154-17169.
25. Y.-P. Liang, Y.-B. Chan, M. Aminuzzaman, M. Shahinuzzaman, S. Djearamane, K. Thiagarajah, S.-Y. Leong, L.-S. Wong and L.-H. Tey, *Catalysts*, 2025, **15**, 275.
26. Y. J. Wong, H. Subramaniam, L. Shing Wong, A. C. T. A. Dhanapal, Y. B. Chan, M. Aminuzzaman, L.-H. Tey, A. K. Janakiraman, S. Kayarohanam and S. Djearamane, *Green Processing and Synthesis*, 2024, **13**, 20240164.
27. Y. B. Chan, M. Aminuzzaman, Y. F. Win, S. Djearamane, L. S. Wong, S. K. Guha, H. Almohammadi, M. Akhtaruzzaman and L.-H. Tey, *Catalysts*, 2024, **14**, 486.
28. Y. B. Chan, M. Aminuzzaman, L.-H. Tey, Y. F. Win, A. Watanabe, S. Djearamane and M. Akhtaruzzaman, *Materials*, 2023, **16**, 5421.
29. Y. B. Chan, M. Aminuzzaman, X.-T. Chuah, K. Li, P. Balu, L. S. Wong, S. K. Guha and L.-H. Tey, *Nanotechnology Reviews*, 2025, **14**, 20250157.
30. J. Manoharan, N. K. Chinnakannu and B. Ranganathan, *Research Journal of Pharmacy and Technology*, 2023, **16**, 4831-4835.



31. N. Nadeem, A. Habib, S. Hussain, A. Sufian, I. Ahmad, F. Noreen, A. Mehmood, F. Ali, K. M. Batoo and M. F. Ijaz, *J Inorg Organomet Polym*, 2025, **35**, 1036-1051.
32. J. Dolai, K. Mandal and N. R. Jana, *ACS Applied Nano Materials*, 2021, **4**, 6471-6496.
33. M. T. Maru, B. A. Gonfa, O. A. Zelekew, S. P. Fakrudeen, H. Ananda Murthy, E. T. Bekele and F. K. Sabir, *Green Chemistry Letters and Reviews*, 2023, **16**, 2232383.
34. S. N. H. Gardezi, M. T. Akhtar, R. Qadir, M. Mustaqeem, S. Batool, A. B. Siddique, H. Alhumade, M. H. Tahir and M. Saadia, *ACS omega*, 2022, **7**, 47755-47763.
35. M. Z. Ishaque, Y. Zaman, Y. Yousaf, M. Shahzad, A. B. Siddique, H. Zaman, S. Ali and N. Ali, *Water, Air, & Soil Pollution*, 2024, **235**, 43.
36. A. Shah, S. Akhtar, F. Mahmood, S. Urooj, A. B. Siddique, M. I. Irfan, M. Naeem-ul-Hassan, M. Sher, A. Alhoshani and A. Rauf, *Surfaces and Interfaces*, 2024, **51**, 104556.
37. A. B. Siddique, M. A. Shaheen, A. Abbas, Y. Zaman, H. M. Amin, M. M. Alam, N. K. Alharbi, F. Alshehri, A. Shami and F. A. Al-Joufi, *International Journal of Environmental Analytical Chemistry*, 2025, 1-23.
38. Z. Khalid, A. Ali, A. B. Siddique, Y. Zaman, M. F. Sibtain, A. Abbas, M. M. Alam and M. S. Alwethaynani, *RSC advances*, 2025, **15**, 16879-16893.
39. K. Mubeen, A. Irshad, A. Safeen, U. Aziz, K. Safeen, T. Ghani, K. Khan, Z. Ali, I. ul Haq and A. Shah, *Journal of Saudi Chemical Society*, 2023, **27**, 101639.
40. A. Ejaz, Z. Mamtaz, I. Yasmin, M. Shaban, A. B. Siddique, M. I. Irfan, A. Ali, S. Muhammad, M. Y. Sameeh and A. Abbas, *Journal of Molecular Liquids*, 2024, **393**, 123622.
41. R. Kaur, M. Suresh, J. López-Vidrier, S. Gutsch, C. Weiss, M. Prescher, L. Kirste, R. Singh, B. Pal and M. Zacharias, *New Journal of Chemistry*, 2020, **44**, 19742-19752.



42. S. Ullah, M. Shaban, A. B. Siddique, A. Zulfiqar, N. S. Lali, M. Naeem-ul-Hassan, M. I. Irfan, M. Sher, M. F. ur Rehman and A. Hanbashi, *Journal of Environmental Chemical Engineering*, 2024, **12**, 113350.
43. S. Kamble, S. Agrawal, S. Cherumukkil, V. Sharma, R. V. Jasra and P. Munshi, *ChemistrySelect*, 2022, **7**, e202103084.
44. Y. Zaman, M. Z. Ishaque, K. Waris, M. Shahzad, A. B. Siddique, M. I. Arshad, H. Zaman, H. M. Ali, F. Kanwal and M. Aslam, *Arabian Journal of Chemistry*, 2023, **16**, 105230.
45. J. O. Ighalo, P. A. Sagboye, G. Umenweke, O. J. Ajala, F. O. Omoarukhe, C. A. Adeyanju, S. Ogunniyi and A. G. Adeniyi, *Environmental Nanotechnology, Monitoring & Management*, 2021, **15**, 100443.
46. P. Jayaram, P. Pradyumnan and S. Z. Karazhanov, *Physica B: Condensed Matter*, 2016, **501**, 140-145.
47. A. B. Siddique, M. A. Shaheen, S. Shafeeq, A. Abbas, Y. Zaman, M. Z. Ishaque and M. Aslam, *Materials Advances*, 2025.



Availability of data and materials

All evaluated data is available in the manuscript. Additional information/data can be provided upon reasonable request.

